Stokes and anti-Stokes Raman spectra of small-diameter isolated carbon nanotubes

A. G. Souza Filho*
Departamento de Física, Universidade Federal do Ceará, Fortaleza-CE 60455-760, Brazil

S. G. Chou,[1] Ge. G. Samsonidze,[2] G. Dresselhaus,[3] and M. S. Dresselhaus[2,4]
[1]*Department of Chemistry,*
[2]*Department of Electrical Engineering and Computer Science,*
[3]*Francis Bitter Magnet Laboratory,*
[4]*Department of Physics,*
Massachusetts Institute of Technology, Cambridge, Massachusetts 02139-4307, USA

Lei An and J. Liu
Department of Chemistry, Duke University, Durham, North Carolina 27708, USA

Anna K. Swan,[5] M. S. Ünlü,[5] and B. B. Goldberg[5,6]
[5]*Electrical and Computer Engineering Department,*
[6]*Physics Department,*
Boston University, Boston, Massachusetts 02215, USA

A. Jorio
Departamento de Física, Universidade Federal de Minas Gerais, Belo Horizonte, Minas Gerais 30123-970 Brazil

A. Grüneis and R. Saito
Department of Physics, Tohoku University
and CREST, JST, Sendai 980-8578, Japan

(Received 10 May 2003; revised manuscript received 29 September 2003; published 26 March 2004)

By measuring the anti-Stokes (AS) and Stokes (S) Raman spectra on the same isolated single-wall carbon nanotube (SWNT), we here determine the electronic transition energies E_{ii} experimentally (E_{ii}^{exp}), and then we compare these E_{ii}^{exp} with the E_{ii} values obtained with theoretical predictions (E_{ii}^{cal}). In such an approach, the nanotube (n,m) structure identification depends on the theory parameters, but the experimental determination of E_{ii}^{exp} does not, and depends only on the experimental AS/S intensity ratio and the laser energy E_{laser} used in the experiment. We measured the radial breathing mode frequency ω_{RBM} and E_{ii}^{exp} for specific tubes, and we then performed the (n,m) identification by using the d_t diameter dependence of the electronic transitions. We present such an analysis for a wide nanotube diameter range, focusing primarily on small diameter SWNTs ($d_t<1.1$ nm), where there are very few (n,m) possibilities for SWNTs that can be in resonance with the appropriate laser energy E_{laser}. This allows an experimental determination of E_{ii}^{exp} values to be made for a variety of (n,m) SWNTs. Our experimental results indicate that: (i) the large curvature in small diameter tubes induces a σ-π hybridization, thus lowering the electronic band energies, and (ii) the simple formulation of the tight binding model ($\gamma_0=2.89$ eV) to determine E_{ii} starts to deviate from E_{ii}^{exp} for tubes with $d_t<1.1$ nm, but the deviation $\Delta E_{22}=E_{22}^{\mathrm{exp}}-E_{22}^{\mathrm{cal}}$ remains smaller than 20 meV for $d_t\geqslant 0.83$ nm. A comparison between E_{ii}^{exp} data obtained from Raman and photoluminescence is made, and a comparison is also made between E_{ii}^{exp} data for SWNTs and double-wall carbon nanotubes.

DOI: 10.1103/PhysRevB.69.115428 PACS number(s): 77.84.Dy

I. INTRODUCTION

Single-walled carbon nanotubes (SWNTs) are very good prototype materials for modeling one-dimensional systems.[1–3] Clever experiments carried out both on nanotube bundles and single nanotubes have opened up many new opportunities for learning new physical concepts about low-dimensional systems and for checking the validity of theoretical models as well.[1]

The one-dimensional (1D) density of electronic states in SWNTs has been calculated by using the zone folding scheme of the electronic band structure obtained from a tight-binding model for the graphene layer by considering only the occupied π and unoccupied π^* electronic states. The fundamental parameter for connecting experiment and theory in carbon nanotubes to lowest order is the carbon-carbon transfer energy γ_0.[4,5] This lowest-order theory is expected to be approximately valid only for larger diameter tubes ($d_t\geqslant 1.1$ nm). More detailed calculations based on pseudopotential local-density-functional theory have claimed the simple formulation of the tight-binding model to be inaccurate in determining the properties of small-diameter

tubes ($d_t \leqslant 1.1$ nm), because of both the simplifications used in the tight-binding calculations and the hybridization of the σ and π states that arise from the strong curvature effect in these small diameter tubes.[6–8]

Experimental optical absorption and resonance Raman data taken on both SWNT bundles[9] and isolated single-wall nanotubes[10–12] for $d_t \geqslant 1.1$ nm are well explained in terms of a single parameter γ_0. All the Raman spectroscopy results obtained so far at the single nanotube level have been analyzed using a self-consistent approach, and a fitting to the experimental data leads to the $\gamma_0 = 2.89$ eV value.[2] A fundamental ingredient for precisely obtaining the γ_0 parameter is a good experimental assessment of the E_{ii} values. The most quantitative method presently available for accurately measuring the E_{ii} values is through a Raman scattering experiment with a tunable laser. This experiment is very difficult to do and the equipment for carrying out such measurements is generally not available. Such measurements have thus far only been carried out once for isolated nanotubes.[10] An alternative and practical way for obtaining such information is by monitoring the anti-Stokes to Stokes intensity ratio for the radial breathing mode feature in the Raman spectra at a fixed laser energy. The anti-Stokes to Stokes ratio is very sensitive to the position of the laser energy E_{laser} relative to the energy transition E_{ii} because the resonance condition for the scattered photons is different for the anti-Stokes and Stokes process.

Recent methods for the synthesis of SWNTs, either by using identical metal-containing molecular nanoclusters as catalysts[13] or solid supported catalyst,[14] allowed the growth of SWNTs with very small diameter and with a narrow diameter distribution. This advance in the growth of isolated SWNTs offers a unique opportunity and motivation for investigating these small diameter tubes in their isolated form grown on a Si/SiO_2 surface. By measuring the anti-Stokes (AS) and Stokes (S) Raman spectra on the same isolated SWNT, we here determine the electronic transition energies E_{ii} experimentally (E_{ii}^{exp}). We then make a comparison between E_{ii}^{exp} and the E_{ii} values obtained with theoretical predictions (E_{ii}^{cal}) in order to identify the (n,m) integer pairs for each nanotube. In such an approach, the (n,m) identification depends on the electronic band calculation, but the experimental determination of E_{ii}^{exp} does not, and depends only on the experimental AS/S intensity ratio and the laser energy E_{laser} used in the experiment. Thus, we can measure ω_{RBM} and E_{ii}^{exp} for specific tubes, and then perform the (n,m) identification by using the d_t diameter dependence of the electronic transitions. The goal of this paper is to perform such an analysis over a wide d_t range, focusing primarily on small diameter SWNTs where there are very few (n,m) possibilities for a SWNT to be in resonance with the appropriate E_{laser}. This procedure allows a determination of E_{ii}^{exp} values to be made for a variety of (n,m) SWNTs, and an assessment to be made of the accuracy/inaccuracy of the tight-binding model calculations by comparing the experimental E_{ii}^{exp} with theoretical E_{ii}^{cal} values, calculated on the basis of the tight-binding model. The results of this comparison demonstrate that the technique is sensitive enough to measure the deviations $\Delta E_{22} = E_{22}^{\text{exp}} - E_{22}^{\text{cal}}$, showing that ΔE_{22} becomes negative for $d_t < 1.1$ nm, but that the deviation ΔE_{22} for E_{22}^{S} remains less than 20 meV for $d_t \geqslant 0.83$ nm.

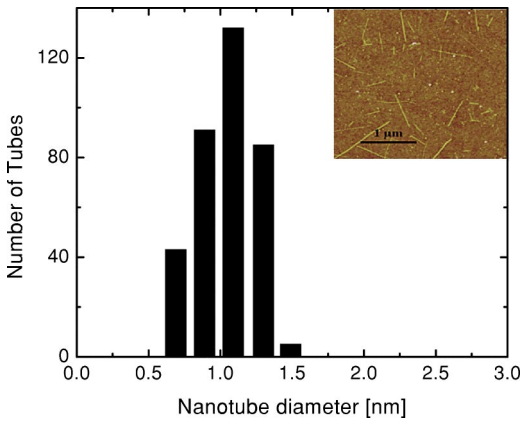

FIG. 1. Diameter distribution of a sample of isolated individual SWNTs on a Si/SiO_2 substrate obtained by atomic force microscopy (AFM) using the method reported in Ref. 13. The inset (upper right) depicts an AFM image of the sample.

II. EXPERIMENT

The isolated tubes used in this paper were prepared by using a chemical vapor deposition (CVD) method on a Si/SiO_2 substrate. Silicon wafers with thin films of thermally grown SiO_2 (about 1 μm thick) were soaked for 30 min in a 0.5 mM methanol solution of 3-aminopropyltriethoxysilane. The wafers were rinsed with isopropanol and blown dry with 1,1,1,2 tetrafluoroethane, and then were kept at 120 °C for a minimum of two hours. The Fe/Mo nanoclusters (prepared by the method described in Ref. 13) were deposited on the chemically modified surfaces by soaking the silicon wafers in the nanocluster solutions for 10 min. The samples were then sonicated in ultrapure water immediately after being taken out of the nanocluster solution to get rid of the physically absorbed nanoclusters, and the samples were then blown dry with 1,1,1,2 tetrafluoroethane.

The wafers were then put into a quartz tube in a furnace. They were first annealed in air for 5 min at 700 °C, and then H_2 (200 sccm) was used to reduce the substrates for 5 min at 900 °C. Subsequently CVD was performed with the mixture of CO (800 sccm) and H_2 (200 sccm) for 15 min at the same temperature. Finally, the system was cooled under an H_2 atmosphere. Atomic force microscopy (AFM) images have shown that our samples have nanotubes with diameters varying from 0.7 to 1.5 nm (for samples grown by the above described method) with an average diameter of about 1.0 nm (see Fig. 1). Samples with larger diameter nanotubes ($d_t > 1.0$ nm) were prepared as described in Ref. 15.

The spectral excitation for resonance Raman experiments was provided by laser lines of $E_{\text{laser}} = 1.58$, 1.96, and 2.41 eV, all of them with a power level $P \leqslant 10$ mW [power density ~ 1 MW/cm^2] at the sample surface. The scattered light was analyzed using a Kaiser Hololab system (for 1.58 eV laser excitation) and a Renishaw 1000 B system (for 1.96

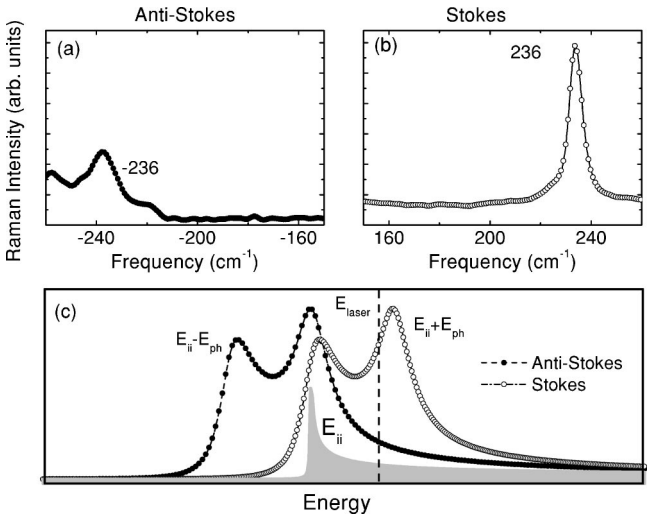

FIG. 2. (a) Anti-Stokes and (b) Stokes radial breathing mode Raman spectra for a semiconducting (10,5) tube as identified in this work. The anti-Stokes spectrum intensity is normalized with the Boltzmann factor. (c) Resonant window for both the normalized anti-Stokes (solid circles) and Stokes (open circles) Raman processes. The gray plot stands for the joint density of states profile for a given tube. The laser energy is represented as a vertical dashed line.

and 2.41 eV laser excitations), both equipped with a cooled charge-coupled device (CCD) for detecting the scattered light.

Both Stokes and anti-Stokes spectra are taken simultaneously and so the time acquisition and laser power are the same for both spectra. For the purpose of this paper, it is the anti-Stokes to Stokes intensity ratio that is the fundamental quantity that is measured. For using this experimental input properly, we first correct the measured intensity for the instrumental response at different wavelengths by accounting for the efficiencies of the gratings and the detector efficiencies. Second, we normalized the anti-Stokes signal by the Boltzmann factor $\exp[-E_{\mathrm{ph}}/kT]$, where E_{ph} is the phonon energy. Since no evidence for overheating the SWNTs was observed experimentally when the laser power level was varied, a sample temperature of 300 K was considered in this normalization procedure. After taking account of these two factors that greatly affect the anti-Stokes to Stokes intensity ratio, the observed asymmetry in the phonon intensity for the anti-Stokes and Stokes spectra [see Fig. 2(c)] comes from the difference in the resonant conditions between the incident and scattered photons with the electronic transitions, which is the physics that is used to determine E_{ii} experimentally.

III. RESULTS AND DISCUSSION

A. E_{ii} determination from anti-Stokes/Stokes ratio

In Figs. 2(a) and 2(b) we show the Raman spectra for an isolated SWNT identified in this work as (10,5) whose RBM frequency is 236 cm^{-1}. In this figure the anti-Stokes intensity is normalized by the Boltzmann factor to account for the temperature dependence of the phonon population. In an ordinary Raman scattering experiment (*off resonance*) carried out at room temperature, the Stokes intensity is larger than the anti-Stokes intensity. However, after the normalization procedure that takes the Boltzmann factor into account, the normalized anti-Stokes to Stokes intensity ratio under *off resonance* conditions is always 1. In the case where the experiment is carried out *on resonance*, as is done for SWNTs, the anti-Stokes to Stokes intensity ratio is equal to 1 when $E_{ii} \sim E_{\mathrm{laser}}$. The asymmetry observed in Figs. 2(a) and 2(b) can be understood by considering the resonance process. For this particular SWNT spectrum, one can observe that the Stokes intensity is larger than that of the anti-Stokes intensity. This occurs because the resonance process is not only due to the incident photon, but there is also a resonance with the scattered photon. The scattered photons have different energies for the Stokes and anti-Stokes processes, and these energies are, respectively, $E_{\mathrm{laser}}-E_{\mathrm{ph}}$ and $E_{\mathrm{laser}}+E_{\mathrm{ph}}$. Then for a given phonon, such as for the RBM phonon shown in Figs. 2(a) and 2(b), there are two resonant peaks for the Stokes process and two peaks for the anti-Stokes process, as shown for the calculated line shapes in Fig. 2(c). One of these peaks is common to both processes, and occurs when $E_{\mathrm{laser}}=E_{ii}$ corresponding to the resonance with the incident photons. For the other resonant peaks, this condition is downshifted (upshifted) by the phonon energy in the case of the anti-Stokes (Stokes) process and the peak occurs when $E_{\mathrm{laser}}=E_{ii}-E_{\mathrm{ph}}$ ($E_{\mathrm{laser}}=E_{ii}+E_{\mathrm{ph}}$). The intensity of a given phonon for both the Stokes and the normalized anti-Stokes spectra as a function of laser energy was experimentally obtained through an experiment with a tunable laser[10] and this profile [referring to the plot in Fig. 2(c)] was used here for analyzing the anti-Stokes to Stokes intensity ratio.

By analyzing the line shape in Fig. 2(c) we can see that the anti-Stokes (solid circles) to Stokes (open circles) intensity ratio depends sensitively on the position of the laser energy [vertical dashed line in Fig. 2(c)] relative to the singularity E_{ii}. If $E_{\mathrm{laser}}>E_{ii}$, the Stokes spectrum is more intense than its anti-Stokes counterpart, as in the case of Figs. 2(a) and 2(b). If $E_{\mathrm{laser}}<E_{ii}$, the Stokes spectrum is less intense than its anti-Stokes counterpart, considering the normalization of the experimental data by the Boltzmann factor in Fig. 2(a). The special situation, where both Stokes and anti-Stokes processes have about the same resonance enhancement factor, occurs when $E_{\mathrm{laser}} \sim E_{ii}$. The dependence of the anti-Stokes to Stokes intensity ratio on laser energy allows one to use the measured ratio of the anti-Stokes to Stokes intensities I_{AS}/I_S for the radial breathing mode for a given E_{laser} to sensitively determine the energy E_{ii} of the resonant van Hove singularity in the joint density of states.[11] This determination is done by adjusting the experimental E_{ii}^{exp} which would produce the measured I_{AS}/I_S ratio for that particular (n,m) tube when using a particular E_{laser}. The (n,m) indices were then determined as the best fit of the nanotube diameter d_t (measured from the RBM frequency) and E_{ii}^{exp} to the predicted d_t and E_{ii}^{cal} values [that follow from the (n,m) indices].

B. (n,m) assignments

We have measured both Stokes and anti-Stokes spectra for a number of tubes [20 different (n,m)] in the diameter

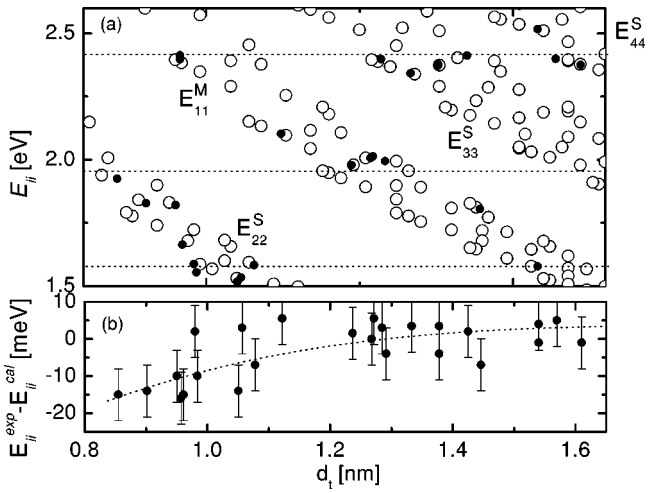

FIG. 3. (a) Experimental (solid symbols) and calculated (open symbols) electronic transitions energies E_{22}^S, E_{33}^S, E_{44}^S, and E_{11}^M for isolated SWNTs probed with different laser energies. The horizontal dashed lines denote the 1.58, 1.96, and 2.41 eV laser energies used in the experiments. (b) Energy difference ΔE_{ii} between experimental and calculated E_{ii} values. The dotted line in (b) is a guide to the eyes.

range 0.83–1.7 nm. We have analyzed the anti-Stokes to Stokes intensity ratio and we have determined the $E_{ii}^{\exp}$ values for each of these nanotubes, including both metallic and semiconducting tubes and the results are summarized in Fig. 3(a). For large diameter tubes ($d_t > 1.1$ nm), we found that the parameter $\gamma_0 = 2.89$ eV is optimal for describing the experimental $E_{ii}^{\exp}$ at the single nanotube level (within a 10 meV range, consistent with experimental deviations), regarding the agreement between $E_{ii}^{\exp}$ and E_{ii}^{cal}. However, as d_t gets smaller than 1.1 nm, some deviations between the calculated and experimentally determined values start to emerge, as can be clearly seen in the trend of the $\Delta E = E_{ii}^{\exp} - E_{ii}^{\text{cal}}$ vs. d_t plot depicted in Fig. 3(b). By taking into account the uncertainties related to the experimental setup and normalization procedure, we conclude that the accuracy for the solid points in Fig. 3 is about 10 meV.

The association of the observed vibrational spectrum with a particular (n,m) SWNT via resonance Raman spectroscopy data is primarily made based on two considerations: (i) The Raman spectrum is observable only for those nanotubes that have E_{ii} energies close to the laser excitation energy E_{laser} due to resonance enhancement; (ii) The frequency of the radial breathing mode depends on the reciprocal diameter $1/d_t$, and ω_{RBM} is found to depend on $1/d_t$ by the $\omega_{\text{RBM}} = \alpha/d_t$ relation. The value $\alpha = 248$ cm^{-1}nm was determined for isolated nanotubes lying on a Si/SiO_2 surface.[16] By combining information about E_{ii} (resonance enhancement) with the diameter dependence of the radial breathing mode, it is possible to correlate the observed Raman spectral properties with a specific (n,m) SWNT. The observation of a Raman spectrum for an isolated tube means that the laser energy is close to E_{ii}, but from the Stokes spectrum alone, we cannot obtain the precise value of E_{ii}. However, by analyzing the anti-Stokes to Stokes intensity ratio, we can get the value of the resonant E_{ii} singularity quantitatively. This intensity ratio indicates unambiguously whether the laser energy is either above or below the E_{ii} value, as we show in discussing Fig. 2(c). This approach was used to associate each experimental point in Fig. 3 with a given calculated (n,m) SWNT.

For large diameter tubes, sometimes we have more than one possibility for assigning (n,m) pairs for a given Raman spectrum. However, in the small diameter tube range, there are very few possibilities for assigning (n,m) pairs when using a particular E_{laser} line. It is also in the small d_t limit ($d_t < 1.1$ nm) that the tight-binding approximation is expected to be less accurate, as calculations in the literature have pointed out.[6,7] Due to the large curvature for the small d_t SWNTs, the σ states should perturb the π-band electronic levels, and then either more parameters in the Slater-Koster picture or some σ-π band mixing should be added, or both types of corrections should be used for describing the SWNT band structure. Since our method for determining $E_{ii}^{\exp}$ is independent of the band-structure model (the I_{AS}/I_S intensity ratio depends sensitively on the energy of the singularity in the joint density of electronic states), a comparison of the $E_{ii}^{\exp}$ values with the corresponding E_{ii}^{cal} is a good approach to obtain a definite (n,m) tube assignment also for small d_t SWNTs. In Table I, we list all the (n,m) tubes we have identified by the I_{AS}/I_S intensity ratio method, along with their E_{ii} values, as obtained from calculations and from experiments.

By comparing the experimental $E_{ii}^{\exp}$ results (solid circles) with the predicted E_{ii}^{cal} (open circles), we found that the parameters ($\alpha = 248$ cm^{-1}nm, $\gamma_0 = 2.89$ eV) best map each experimental point on to its calculated counterpart. In order to make this clear, we show the calculated and experimental E_{ii} for the large d_t range [covering the E_{33}^S and E_{44}^S transitions in Fig. 4(a)] and the small d_t range [covering the E_{22}^S transition in Fig. 4(b)]. The E_{ii}^{cal} for which we assigned experimental values for $E_{ii}^{\exp}$ are marked by open circles enclosing "+" signs. By inspecting Fig. 3(b), one can see (Table I) a trend in the deviation between the experimental $E_{ii}^{\exp}$ values and those calculated by the tight binding model E_{ii}^{cal}, namely, that the deviation $\Delta E_{ii} = (E_{ii}^{\exp} - E_{ii}^{\text{cal}})$ becomes more negative as d_t gets smaller, thus indicating that the tight-binding approximation *overestimates* the van Hove singularity energies for small-diameter tubes. *Ab initio* calculations of the nanotube electronic structure have indicated that nanotube curvature induces a σ-π hybridization, thus *lowering* the electronic band energies.[6,7,17] This picture is qualitatively consistent with our experimental results shown in Fig. 3. In Table I, we list all the (n,m) tubes we have identified by the I_{AS}/I_S intensity ratio method, along with their E_{ii} values, as obtained from calculations and from experiments. However, we should emphasize that the deviations from the tight-binding calculations that we have observed experimentally are on the order of 20 meV or less. These deviations are much smaller than the numerical precision achieved in *ab initio* calculations (around 100 meV) and much smaller than the magnitude of their predicted deviations from the tight-binding calculations (50 meV).

TABLE I. Assigned (n,m) and E_{ii}^{exp} using the measured anti-Stokes to Stokes intensity ratio for isolated SWNTs and $\gamma_0 = 2.89$ eV. Also shown are E_{ii}^{cal} obtained from (n,m) by tight binding calculations and the deviation energy $\Delta E_{ii} = E_{ii}^{\mathrm{exp}} - E_{ii}^{\mathrm{cal}}$.

(n,m)	d_t(nm)	θ	$\omega_{\mathrm{RBM}}(\mathrm{cm}^{-1})$		E_{ii}(eV)		ΔE(meV)
			Exp.	$248/d_t$	Calc.	Exp.	
					E_{11}^{M} [a]		
(12,0)	0.95	8.2	259	261	2.413	2.397	−16
(9,9)	1.24	30	201	200	1.977	1.979	2
(12,6)	1.26	19.1	196	197	2.007	2.007	0
(16,1)	1.31	3	192	195	1.998	1.994	−4
(14,8)	1.53	21.1	161	162	1.577	1.578	1
					E_{22}^{S}		
(17,2)	1.44	5.5	172	173	1.812	1.806	−6
(11,5)	1.13	17.8	221	220	2.097	2.103	6
(11,4)	1.07	14.9	230	232	1.594	1.583	−9
(10,5)	1.05	19.1	236	237	1.531	1.517	−14
(11,3)	1.01	11.7	252	245	1.564	1.554	−10
(12,1)	0.99	4.0	253	250	1.585	1.587	2
(7,6)	0.86	27.5	277	275	1.841	1.827	−14
(7,5)	0.83	24.5	288	298	1.940	1.925	−15
					E_{33}^{S}		
(14,6)	1.41	17.0	173	175	2.410	2.412	2
(11,9)	1.38	26.7	180	179	2.373	2.377	4
(13,6)	1.34	18.0	186	185	2.339	2.341	2
(15,2)	1.28	6.2	194	194	2.395	2.398	3
					E_{44}^{S}		
(18,4)	1.61	11.9	154	154	2.376	2.375	−1
(15,7)	1.55	18.1	162	160	2.506	2.509	3
(20,0)	1.59	0.0	158	159	2.394	2.399	5

[a]The values listed stand for the lower-energy component of the E_{11}^{M} singularity, whereas there is only one component for the semiconducting E_{22}^{S}, E_{33}^{S}, and E_{44}^{S} singularities for a given tube.

C. Comparison with other experiments

1. Comparison between isolated and bundled SWNT Raman data

In order to further check the validity of using the $\omega_{\mathrm{RBM}} = 248/d_t$ relation for interpreting our results, we have employed the method developed by Kuzmany *et al.*[18] that allows one to evaluate the diameter distribution of the tubes in a SWNT bundle by using the RBM spectral response. The fundamental ingredients used in this method[18] are the first and second moments of the RBM distribution. In Ref. 18 the analysis is carried out using the relation $\omega_{\mathrm{RBM}} = 234/d_t + \beta$, where β is a term that has been described to account for tube-tube interactions and its values are obtained by fitting the experimental RBM data. The 234 factor is the value obtained from an *ab initio* calculations and this value was also considered by Kuzmany *et al.* to be an optimal value for this parameter. We have analyzed our data by considering the general equation $\omega_{\mathrm{RBM}} = \alpha/d_t + \beta$ and we have used our isolated tube data as follows. We summed up the various spectra obtained for isolated tubes to get a *bundle-like* spectra. In so doing, we can apply the method described in Ref. 18 to analyze our data. By fitting the first and second moment calculated for our RBM spectral profile, we obtained $\alpha = 251.12$ nm cm^{-1} and $\beta = -1.13$ cm^{-1}. Since the magnitude of α is the same as the experimental accuracy (~ 2 cm^{-1}), we can consider $\beta = 0$ (as expected, since there is no tube-tube interaction), thus implying that the $\alpha = 251.12$ nm cm value confirms the validity of using the 248 ± 4 nm cm^{-1} constant that we have established for isolated tubes sitting on a Si/SiO_2 substrate.[2]

2. Raman vs photoluminescence data

Optical absorption and photoluminescence data have also been used to determine E_{ii} values for semiconducting SWNTs.[14,19–22] We also plot, for comparison, the experimental E_{ii} values [open triangles in Fig. 4(b)] for the E_{22}^{S} transition obtained through optical absorption of isolated SWNTs dispersed in a solution.[19,20] The kinds of isolated tubes that have been studied by optical absorption[19–22] are different from the samples we have investigated in the present Raman scattering studies (isolated SWNTs sitting on a Si/SiO_2 surface). The SWNTs for the optical experiments are obtained by dispersing SWNT bundles with an ultracentrifuge into isolated SWNTs surrounded by the surfactant sodium dodecyl sulfate (SDS), thus forming micelles around each SWNT. As can be clearly observed in Fig. 4(b), the transition ener-

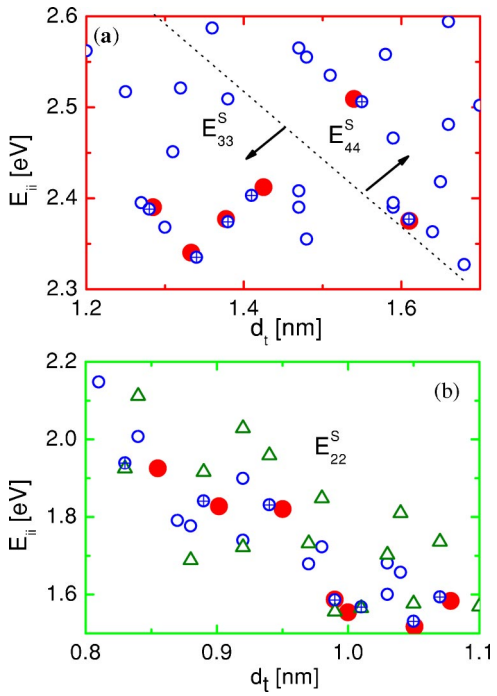

FIG. 4. Experimental (solid circles) and calculated (open circles) electronic transition energies E^S_{22} (lower panel), E^S_{33} and E^S_{44} (upper panel), for isolated single-wall nanotubes. The circles enclosing "+" signs stand for $E^{\rm cal}_{ii}$ for the nanotubes for which we have assigned $E^{\rm exp}_{ii}$ (solid circles) values. In the lower panel the open triangles stand for data obtained from photoluminescence spectroscopy taken from Ref. 20.

gies reported by Bachilo *et al.*[20] deviate from both our calculated and experimental data beyond our measured uncertainties. It is not surprising that the results for these two distinctly different experiments are different, because Bachilo *et al.*[20] have established for their sample a different d_t dependence for their $\omega_{\rm RBM}$ (in units of $\rm cm^{-1}$), namely, $\omega_{\rm RBM}=223/d_t+12.5$. We, in fact, tried to use this d_t dependence for $\omega_{\rm RBM}$ to fit our $E^{\rm exp}_{ii}$ data (that are determined from Raman spectra, independent of any band calculation). In so doing, we could not observe a match between our $E^{\rm exp}_{ii}$ data with the modified $E^{\rm cal}_{ii}$ values (calculated from tight binding) for the Bachilo *et al.*[20] data, and based on their values of d_t. From this exercise, we concluded that our diameter dependence $\omega_{\rm RBM}=248/d_t$ can account for our experimental Raman results and that the $\omega_{\rm RBM}=223/d_t+12.5$ expression does not fit our experimental results. This comparison suggests that each kind of sample has its own parameters in relating $\omega_{\rm RBM}$ and d_t, and perhaps each kind of sample also has different $E^{\rm exp}_{ii}$ values. It therefore seems to be very difficult at the present time to unify all of these data quantitatively, because of the different interactions between the nanotube species and their local environments. Future studies of the optical spectra and the analysis of the normalized anti-Stokes to Stokes intensity ratio of the Raman spectra from the *same isolated individual* SWNT should shed further light on why different expressions for $\omega_{\rm RBM}$ are needed for the interpretation of these complementary experiments.

Another result reported by Bachilo *et al.*[20] is that the E^S_{22}/E^S_{11} ratio is significantly smaller than the value of 2, the latter which would be expected to apply on average, based on the simple theoretical framework that we have used to analyze our Raman data. It is also remarkable that the spread in the E^S_{22} energies obtained from photoluminescence [see open triangles in Fig. 4(b)] is much greater than that observed experimentally from Raman spectroscopy at the single nanotube level and found theoretically from tight-binding calculations. Deviations of E^S_{22}/E^S_{11} on average from the expected ratio of 2 is referred to as the "ratio problem" and could perhaps be due to exciton effects. One would expect excitons to mainly affect the E^S_{11} transitions. We emphasize here that the E^S_{22} values determined by Bachilo *et al.*[20] fall into the same energy range as our E^S_{22} [see Fig. 4(b)] values, and that our E^S_{22} values do not deviate from the tight-binding energies by more than 20 meV for $d_t>0.83$ nm [see Fig. 4]. The results of our work imply that a negative deviation in the E^S_{22}/E^S_{11} ratio from 2 must be due to an *upshift* in the E^S_{11} energies that are reported for photoluminescence measurements when compared with tight-binding calculations. Normally exciton effects would be expected to *downshift* E^S_{11} energies, making the implied *upshift* in E^S_{11} from photoluminescence measurements so interesting. A recent report by Kane and Mele[23] has pointed out that many-body excitations are responsible for perturbing the energy bands and that many body effects can also upshift E^S_{11}.

A recent paper by Sakai *et al.*[24] reports that the E_{ii} separation is increased from a simple one-electron energy when the electron-electron repulsion interaction is taken into account. Generally, it is expected that an exciton effect between the electron and the hole (attractive potential) lowers the E_{ii} values. In low-dimensional materials, the lowest-energy separation $i=1$ is expected to give the largest exciton effect. But in the case of carbon nanotubes according to Sakai *et al.*[24] a rather different behavior should be observed. The lowest E_{11} energy was found to have a smaller binding energy[24] for the exciton than the higher-energy transitions owing to its smaller effective mass. Thus the E_{11} energy values are slightly upshifted compared with the other E_{ii} values, and the E^S_{22}/E^S_{11} ratio being smaller than 2 is thus explained by these authors.[24] The theory discussed in Ref. 24 also elucidates the different γ_0 values determined from optical and scanning probing microscopy. The $\gamma_0=2.9$ eV determined for explaining the optical experiments includes many body effects, in contrast to $\gamma_0=2.6$ eV, determined from scanning-tunneling microscopy experiments. Basically, the results of Fig. 4 imply that the photoluminescence spectra are suggesting a larger trigonal warping effect than what is found from analysis of Raman spectra at the single nanotube level.

Recent simultaneous Raman Stokes and photoluminescence experiments done on the same isolated nanotube has added new considerations to the "ratio problem" scenario and also to the emission properties of SWNTs.[25] Firstly, Hartschuh *et al.*[25] found that (6,4) and (6,5) nanotubes pumped to the first excited state exhibit the same fluorescence energy as the energy observed by Bachillo *et al.*[20] for

the same tubes but excited to the second state. The results obtained by Hartschuh *et al.*[25] suggested that the many electron picture seems to fail in explaining emission properties of small diameter tubes. Even though the ratio problem has been discussed extensively in the literature, this problem and its various manifestations have not yet been resolved either experimentally or theoretically. Secondly, the authors of Ref. 25 also observed that two SWNTs with identical Raman spectra also exhibit considerably different emission spectra regarding the position of the emission energy. For the (7,5) tube Hartschuh *et al.*[25] get peak values for E_{11}^{S} emission measurements ranging from 1.21 to 1.23 eV. This result points out that the peak positions in the PL data are very sensitive to the local environment and this should be the reason why, up to now, it has been very difficult to establish a clear picture in correlating the photophysics results from different samples and techniques.

3. Isolated SWNTs vs double-wall nanotubes

Regarding small diameter tubes, we now compare our data for isolated SWNTs with those reported for double-wall nanotubes whose inner tubes are very small in diameter. Recently, Kramberger *et al.*[26] have observed well-resolved features in the Raman spectra of double-wall nanotube bundle samples for the small diameter range (<1 nm) and, they assign a large set of (n,m) indices to observed Raman features for the inner tubes of the double-wall species. Most of the inner tubes assigned in Ref. 26 fall in a lower diameter range compared with the tubes that we list in Table I. Furthermore, they observed many more tubes than are reported in Table I, because their experiments were carried out on a bundle sample, whereby all of the possible chiralities for a given diameter range are presumably present. However, some of the tubes that we assign are also on the list of the inner tubes observed for double-wall tubes.[26] Good agreement between the structural data for the (12,0), (11,3), and (7,6) tubes is indeed observed. Small discrepancies in the RBM frequencies come from the different equations used for correlating the ω_{RBM} with the tube diameter d_t. In the case of double-walled nanotubes, small changes in the RBM frequency for the inner tube compared with its SWNT counterpart are expected due to the presence of the outer tube. The assignments carried out for the inner tubes in Ref. 26 are based on a equation $\omega_{\mathrm{RBM}}=\alpha/d_t+\beta$, while we have found from fitting our data for the tubes sitting on Si/SiO_2 substrate that β is negligibly small. Stokes to anti-Stokes intensity ratio measurements on double wall nanotubes would allow one to make a more accurate assessment of the chiralities and to improve the models for precisely correlating specific (n,m) tubes with specific spectral features.

IV. CONCLUSIONS

In summary, we have presented an analysis of the Stokes and anti-Stokes Raman spectra for isolated single-wall carbon nanotubes. We have focused our analysis on small-diameter tubes where few possibilities are found for assigning (n,m) pairs to the observed Raman spectra. The measured normalized anti-Stokes to Stokes intensity ratio I_{AS}/I_S is used for obtaining the electronic transition energies E_{ii}^{exp}, independent of band-structure calculations. By comparing the E_{ii}^{exp} with E_{ii}^{cal} values calculated from a tight-binding model on a one-on-one basis, we have made (n,m) pair assignments, and we have found that the deviation between experiment and tight-binding theory $\Delta E_{ii}=E_{ii}^{\mathrm{exp}}-E_{ii}^{\mathrm{cal}}$ does indeed depend on d_t. The deviation ΔE_{ii} is observed to become more negative as the tube diameter gets smaller, thus indicating that the tight-binding approximation *overestimates* the van Hove singularity energies for small d_t tubes ($0.8<d_t<1.1$ nm). Our experimental results indicate that: (i) the large curvature in the small diameter tubes, which induces a σ-π hybridization, lowers the electronic band energies, and (ii) the simple formulation of the tight binding model to determine E_{ii} is accurate to 20 meV for tube diameters larger than 0.83 nm. Finally it should be pointed out that the ability to grow SWNTs with a very narrow diameter distribution is rapidly increasing.[27] This will allow more systematic and precise connections to be made between experiments and models since these special samples will contain only a small number of different (n,m) SWNTs.

ACKNOWLEDGMENTS

The authors gratefully acknowledge Professors J.H. Hafner and C.M. Lieber, who provided the samples for carrying out the single nanotube spectroscopy measurements on larger diameter SWNTs. The authors also acknowledge Professors M.A. Pimenta and J. Mendes Filho for valuable discussions related to this work. The authors A.G.S.F. and A.J. acknowledge financial support from the Brazilian agencies CAPES (PRODOC grant) and CNPq (Profix grant), respectively. Part of the experimental work was performed at Boston University at the Photonics Center, operated in conjunction with the Boston University Department of Physics and the Department of Electrical and Computer Engineering. The MIT authors acknowledge support from the Dupont-MIT alliance and NSF Grant DMR 01-16042. This work also made use of the MRSEC Shared Facilities at MIT, supported by the National Science Foundation under Grant No. DMR-9400334 and NSF Laser facility Grant No. 97-08265-CHE. R.S. acknowledges a Grant-in-Aid (Grant No. 13440091) from the Ministry of Education, Japan. The authors gratefully acknowledge the NSF/CNPq joint collaboration program (NSF Grant No. INT. 00–00408 and CNPq Grant No. 910120/99-4). The authors from Duke University acknowledge support from NASA (NAG-1-01061).

*Electronic address: agsf@fisica.ufc.br

[1] For an updated review see, M.S. Dresselhaus, G. Dresselhaus, and P. Avouris, *Carbon Nanotubes: Synthesis, Structure, Properties and Applications*, Springer Series in Topics in Applied Physics, Vol. 80 (Springer-Verlag, Berlin, 2001).
[2] M.S. Dresselhaus, G. Dresselhaus, A. Jorio, A.G. Souza Filho, and R. Saito, Carbon **40**, 2043 (2002).
[3] Acc. of Chem. Res **35** (2002), Special issue on Single-Wall Carbon Nanotubes, edited by R. Haddon.
[4] R. Saito, M. Fujita, G. Dresselhaus, and M.S. Dresselhaus, Appl. Phys. Lett. **60**, 2204 (1992).
[5] J.W. Mintmire, B.I. Dunlap, and C.T. White, Phys. Rev. Lett. **68**, 631 (1992).
[6] X. Blase, L.X. Benedict, E.L. Shirley, and S.G. Louie, Phys. Rev. Lett. **72**, 1878 (1994).
[7] D.S. Portal, E. Artacho, J.M. Soler, A. Rubio, and P. Ordejón, Phys. Rev. B **59**, 12 679 (1999).
[8] I. Cabria, J.W. Mintmire, and C.T. White, Phys. Rev. B **67**, 121406(R) (2003).
[9] M.S. Dresselhaus and P.C. Eklund, Adv. Phys. **40**, 705 (2000).
[10] A. Jorio, A.G. Souza Filho, G. Dresselhaus, M.S. Dresselhaus, R. Saito, J.H. Hafner, C.M. Lieber, F.M. Matinaga, M.S.S. Dantas, and M.A. Pimenta, Phys. Rev. B **63**, 245416 (2001).
[11] A.G. Souza Filho, A. Jorio, J.H. Hafner, C.M. Lieber, R. Saito, M.A. Pimenta, G. Dresselhaus, and M.S. Dresselhaus, Phys. Rev. B **63**, 241404(R) (2001).
[12] Z. Yu and L.E. Brus, J. Phys. Chem. B **105**, 1123 (2002).
[13] L. An, J.M. Owens, L.E. McNeil, and J. Liu, J. Am. Chem. Soc. **124**, 13688 (2002).
[14] S.M. Bachilo, L. Balzano, J.E. Herrera, F. Pompeo, D.E. Resasco, and R.B. Weisman, J. Am. Chem. Soc. **125**, 11186 (2003).
[15] J.H. Hafner, C.L. Cheung, T.H. Oosterkamp, and C.M. Lieber, J. Phys. Chem. B **105**, 743 (2001).
[16] A. Jorio, R. Saito, J.H. Hafner, C.M. Lieber, M. Hunter, T. McClure, G. Dresselhaus, and M.S. Dresselhaus, Phys. Rev. Lett. **86**, 1118 (2001).
[17] S. Reich, C. Thomsen, and P. Ordejón, Phys. Rev. B **65**, 155411 (2002).
[18] H. Kuzmany, W. Plank, M. Hulman, C. Kramberger, A. Grüneis, T. Pichler, H. Peterlik, H. Kataura, and Y. Achiba, Eur. Phys. J. B **22**, 307 (2001).
[19] M.J. O'Connell, S.M. Bachilo, C.B. Huffman, V.C. Moore, M.S. Strano, E.H. Haroz, K.L. Rialon, P.J. Boul, W.H. Noon, C. Kittrell, J.P. Ma, R.H. Hauge, R.B. Weisman, and R.E. Smalley, Science **297**, 593 (2002).
[20] S.M. Bachilo, M.S. Strano, C. Kittrell, R.H. Hauge, R.E. Smalley, and R.B. Weisman, Science **298**, 2361 (2002).
[21] J. Lefebvre, Y. Homma, and P. Finnie, Phys. Rev. Lett. **90**, 217401 (2003).
[22] M.S. Strano, S.K. Doorn, E.H. Haroz, C. Kittrell, R.H. Hauge, and R.E. Smalley, Nano Lett. **3**, 1091 (2003).
[23] C.L. Kane and E.J. Mele, Phys. Rev. Lett. **90**, 207401 (2003).
[24] H. Sakai, H. Suzuura, and T. Ando, J. Phys. Soc. Jpn. **72**, 1968 (2003).
[25] A. Hartschuh, H.N. Pedrosa, L. Novotny, and T.D. Krauss, Science **301**, 1354 (2003).
[26] C. Kramberger, R. Pfeiffer, H. Kuzmany, V. Zolyomi, and J. Kurti, Phys. Rev. B **68**, 235404 (2003).
[27] J. Liu, Mater. Res. Bull. (to be published 2004).